Normal-Mode-Analysis-Guided Investigation of Crucial Intersubunit Contacts in the cAMP-Dependent Gating in HCN Channels

Farzana Marni, Shengjun Wu, Gaurav M. Shah, Xin-ping Xu, Amber R. Hackett, Changan Xie, Sabisha Shrestha, Lin Liu, Qinglian Liu, and Lei Zhou

Department of Physiology and Biophysics, School of Medicine, Virginia Commonwealth University, Richmond, Virginia

Supplemental Methods

NMA based on all-atom (united) force field or anisotropic network model (ANM)

The PDB file for the mHCN2 CL-CNBD structure (PDB ID: 1Q5O) was cleaned up by removing crystal water molecules and ions (23). Missing atoms and residues were added by Modeller (63). Based on the GROMOS96 43a1 force field, the PDB2GMX program from GROMACS package was used to generate the protein topology file (64). The PRODRG server was used to generate the structure and topology files for cAMP molecules (65). Partial charges for the atoms near the cyclic phosphate group in cAMP were adjusted in reference to each atom's local chemical environment, with the total charge to be -1. For all-atom NMA, we maintained a 5Å layer of explicitly treated water molecules on protein surface (66). To ensure the starting structure at a local energy minimum, three energy minimization steps were sequentially applied at double numerical precision: steepest descent (SD), conjugate gradient (CG), and limited-memory Broyden-Fletcher-Goldfarb-Shanno (L-BFGS). The electrostatic energy was described by a switch function with the distance for normal treatment set at 15Å and the cut-off distance set at 18Å (67). Programs of mdrun_d and g_nmeig_d were used to generate and diagonalize the Hessian matrix, respectively. For ANM-based NMA, C-α atom coordinates were extracted from the energy minimized structure. The Anisotropic Network Model (ANM) program was used with the unified force constant set as 1 kcal/mol/Å^2 and the cutoff distance set as 13Å (68).

After obtaining eigenvectors and corresponding eigenvalues of the Hessian system, we used the following equation to calculate the normalized covariance factor between each pair of atoms (i, j):

$$C_{i,j} = \frac{\sum_{k=1}^{N} \frac{X_i^k \cdot X_j^k + Y_i^k \cdot Y_j^k + Z_i^k \cdot Z_j^k}{\varpi_k}}{\left(\sum_{k=1}^{N} \frac{\left(X_i^k\right)^2 + \left(Y_i^k\right)^2 + \left(Z_i^k\right)^2}{\varpi_k}\right)^{\frac{1}{2}} \cdot \left(\sum_{k=1}^{N} \frac{\left(X_j^k\right)^2 + \left(Y_j^k\right)^2 + \left(Z_j^k\right)^2}{\varpi_k}\right)^{\frac{1}{2}}}$$

, where X, Y, Z represent projections in the eigenvector for each atom, k is the index for eigenvector, ω is the corresponding eigenvalue, and N is the number of eigenvectors involved in the calculation (9, 68). To better suit the goal of systematically surveying all contacts, normalized covariance factor rather than the absolute value of covariance was

used. Normalized covariance factor is also called cross-correlation (16). For NMA based on the all-atom force field (AANMA), the unit of eigenvalue is kJ/mol/nm^2/amu according to the GROMACS definition. The eigenvalue generated from ANM calculation was converted to the Gromacs format by a factor of 32.2 (66).

MD simulation of the WT and mutant mHCN2 C-terminal proteins

A triclinic simulation box was generated around the protein molecule with a gap of 10Å on three dimensions. Point mutations were introduced using Modeller. The simulation box was filled with SPC216 water molecules. The whole system was neutralized by exchanging solvent water molecules with either Na$^+$ or Cl$^-$ ions. After energy minimizations, a position-restrained MD simulation (500 ps) was used to relax and equilibrate the whole simulation system before the standard MD simulation. The following settings were applied: timestep, 2 fs; cut-off distance for short-range neighboring list, 0.9 nm; cut-off distance for Coulomb interactions, 0.9 nm; long-range electrostatics treatment, PME; cut-off distance for VDW interactions, 1.4 nm; constant temperature, 300K by Berendsen coupling with a time constant of 0.1 ps; constant pressure, 1 bar by Berendsen coupling with a time constant of 0.5 ps; bond constraint-algorithm, Lincs.

Protein purification and biochemical binding assays

Construction of pSMT3-mHCN2C plasmid and protein purification of mHCN2 CL-CNBD fragment was described previously (42, 46). QuickChange Site-Directed mutagenesis kit (Stratagene) was used to introduce point mutations. BL21 competent cell was used for protein expression. Protein samples were purified through HisTrap column (affinity chromatography), HiTrap Q and HiTrap S columns (ion exchange chromatography), and HiLoad 16/60 Superdex 75 column (size exclusion chromatography) (GE Healthcare). Finally protein samples were concentrated to >10 mg/ml in a buffer containing 5 mM MES-NaOH and 50 mM NaCl (pH 6.0).

Two equilibrium methods, isothermal titration calorimetry (ITC) and fluorescence anisotropy (FA), were used to measure the cAMP binding affinity. For ITC experiments, 40 μl of cAMP at 1.25 mM was sequentially injected into the sample cell containing the protein sample at 75 μM (iTC200 Microcalorimeter by Microcal). ITC experiments were carried out at 37°C, because at 25°C the binding process involves both heat release and

heat absorbtion which complicates interpretation. FA experiments were carried out at 25°C (BEACON 2000 fluorescecne polarization system). Serially diluted protein samples from 40 µM were mixed with a fluorescent cAMP analog (8-Fluo-cAMP from Biolog) at 10 nM.

Two-electrode voltage-clamp (TEVC), inside-out patch-clamp, and patch-clamp fluorometry

The cDNA clone of mHCN2 channel in pGH vector was kindly provided by Dr. Steven Siegelbaum. Point mutations were introduced by a 2-step PCR method and confirmed by DNA sequencing. Template DNA plasmids were linearized by SphI digestion for in vitro RNA synthesis. *Xenopus* oocytes were used for heterologously expressing WT and mutant mHCN2 channels. Fifty nano gram of cRNA was injected into each oocyte. After 1-2 days of incubation at 17°C, HCN channel current from whole oocytes was recorded by the method of TEVC. After 3 to 4 days of incubation, macroscopic currents could be recorded from excised membrane patches by patch-clamp recording in the inside-out configuration. Recording solution contained (in mM): 110 KCl, 1 $MgCl_2$, 1 EGTA, and 10 HEPES (pH 7.4 adjusted with KOH). All experiments were carried out at room temperature.

It is noticeable that HCN2 channel activates slowly and does not reach equilibrium with the 3-second protocol. Early studies utilizing 10 times longer voltage steps (30 seconds for HCN2 or 75 seconds for HCN4) activated the channel to a level closer to the steady-state (38, 39). Thus, the value of $V_{1/2}$ obtained with voltage steps of 3-second long corresponds to the non steady-state condition and should be more negative than the value under completely equilibrated, steady-state condition. Fully resolving the issue how differently WT and mutant channels are away from the equilibrium, with and without cAMP, requires a series of 30-seconds or even longer voltage-steps applied to the same patch which presents a great technical challenge.

The patch-clamp fluorometry setup was based on an Olympus BX50WI microscope equipped with 60X/1.00 water immersion lens. A 473-nm DPSS laser was used as the excitation light source. The following filter set was used: exciter, D480/30; dichroic mirror, DC505LP; emitter, D510LP. The optical signal was detected by the Cascade 1K EMCCD camera (Photometrics Inc.) and analyzed by the ImageJ software.

TurboReg was used to align the stack of image series. A region of interest (ROI) was selected surrounding the arc of the membrane patch in the recording pipette. ΔF was defined as the mean fluorescence intensity of the ROI with the background intensity subtracted. ΔF values collected along a single voltage step were normalized by the value measured at -40 mV when most channels stay in closed state. Normalized ΔF (ΔΔF) reflects the dynamic change in cAMP binding during channel activation. The fluorescent cAMP analog, 8-NBD-cAMP, was obtained from Biolog.

Supplemental Figures

Figure S1 Covariance matrix based on different pools of eigenvectors.

ANM analysis and covariance matrix construction were processed the same as before.

   (A) Covariance matrix based on the first five eigenvectors of the lowest vibration frequencies. This plot is the same as shown in Fig. 1D.

   (B) Covariance matrix based on the eigenvectors 6 – 10.

   (C) Covariance matrix based on the eigenvectors 11 – 15.

Figure S2 Comparing the contact map of C-α atoms and the NMA-based covariance matrix.

   (A) PROTMAP-2D was used to generate the contact map. The cut-off distance was set as 8Å (http://genesilico.pl/protmap2d.htm). Notice that the results contain only two values, 0 (no contact, black) and 1 (contact, white).

   (B) Contact map generated with the cut-off distance set as 13Å, the same setting as used in ANM analysis.

   (C) Covariance matrix based on ANM analysis. Colors represent different values of covariance factor: red (1 - 0.775), orange (0.775-0.55), yellow (0.55-0.325), and green (0.325-0.1).

Figure S3 Location of K452 and R590 in the crystal structure of CL-CNBD.

(A) K452 is located in the A'-helix in C-linker. R590 is located in the loop between P-helix and β-7 in CNBD. Both residues are in direct contact with residues from neighboring subunits but not with cAMP.

(B) A zoomed view over K452 and E494. The atomic distance between the NZ atom of K452 and the CD atom of R590 is 5.8Å.

(C) A zoomed view over the R590 and E617. The atomic distance between the CZ atom of R590 and the backbone carbonyl oxygen atom of E617 is 3.6Å. The distance between the CZ atom of R590 and the CD atom of E617 is 5.0Å.

Figure S4. Further testing the salt bridge between K452 and E494 by charge swapping.

(A) Representative TEVC traces of mHCN2/R591E and WT mHCN2 channels. Because the R591E mutation abolished cAMP binding, the difference between R591E and WT traces reflect the cAMP-dependent regulation of channel gating.

(B) TEVC traces of K452E mutant channel and K452E+E494R double mutant channel.

(C) Summary of resting $V_{1/2}$ values. The positive shift of about +11mV in $V_{1/2}$ between R591E and WT channels reflects the contribution from the cAMP-dependent gating. Independent t-test shows that the K452E channel is significantly different from WT channel ($p<0.001$). The channel carrying double point mutation K452E+E494R is not different from WT channel ($p=0.31$).
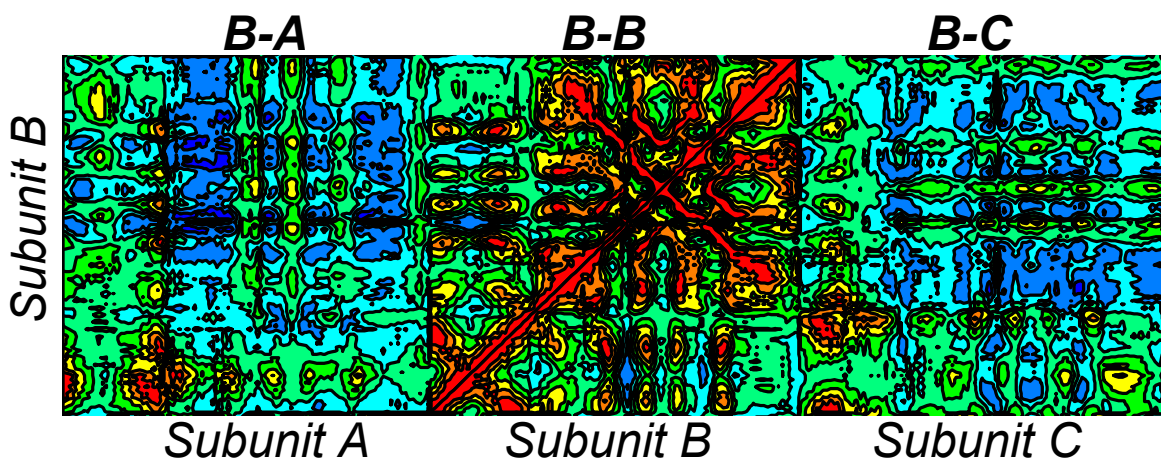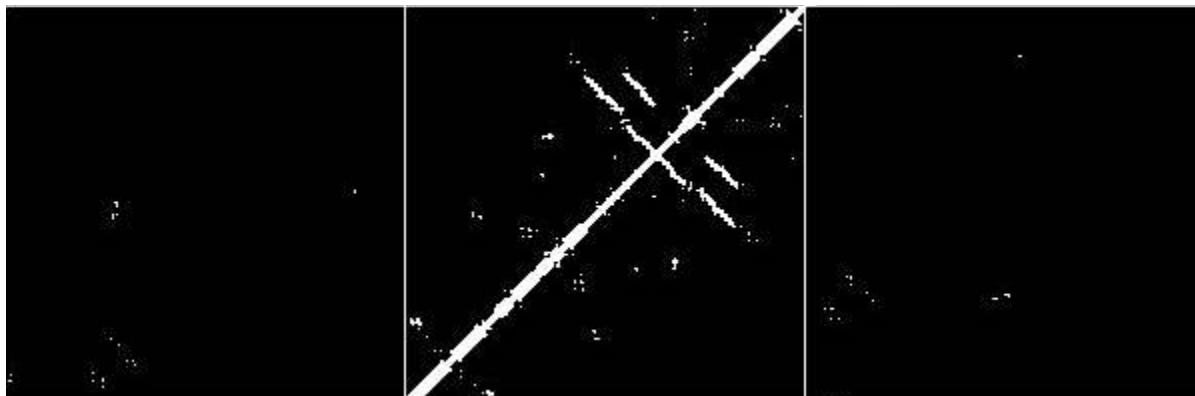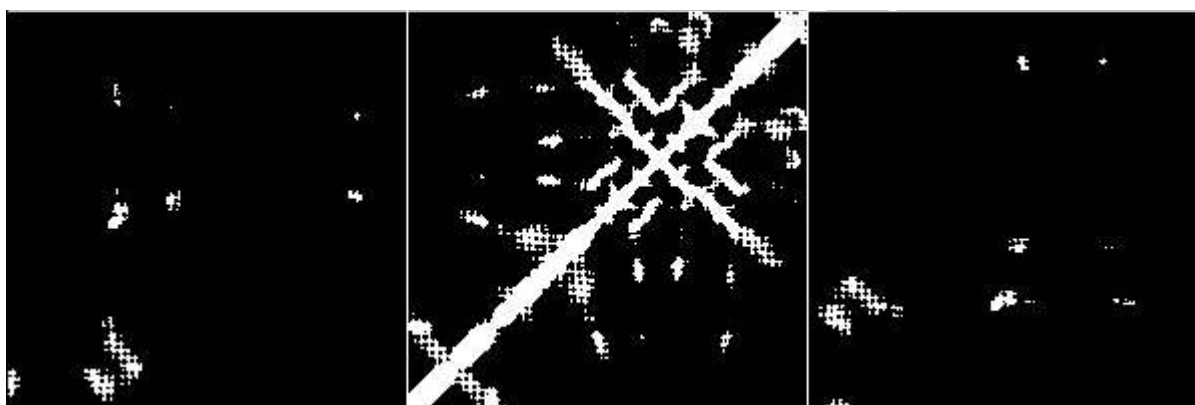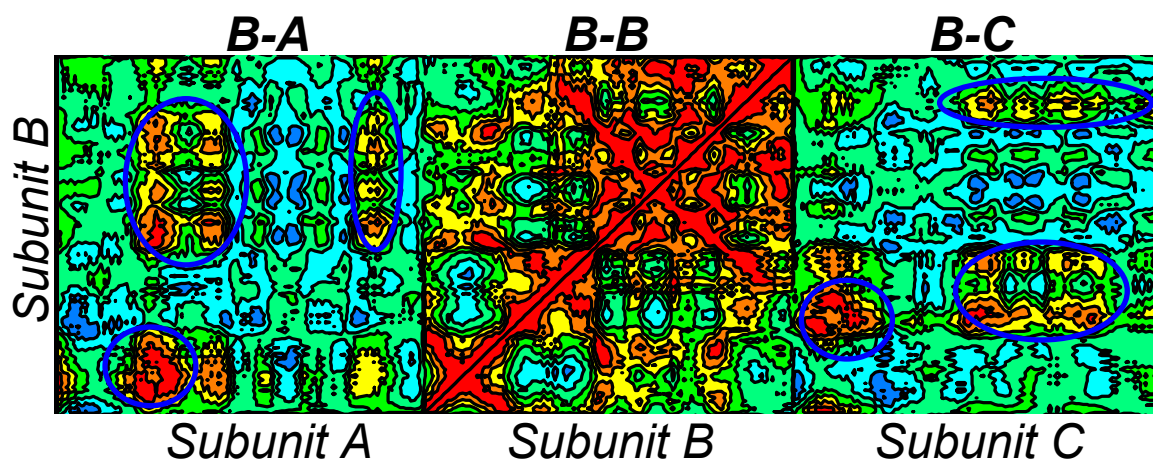
A ANM analysis (eigenvector 1 to 5)
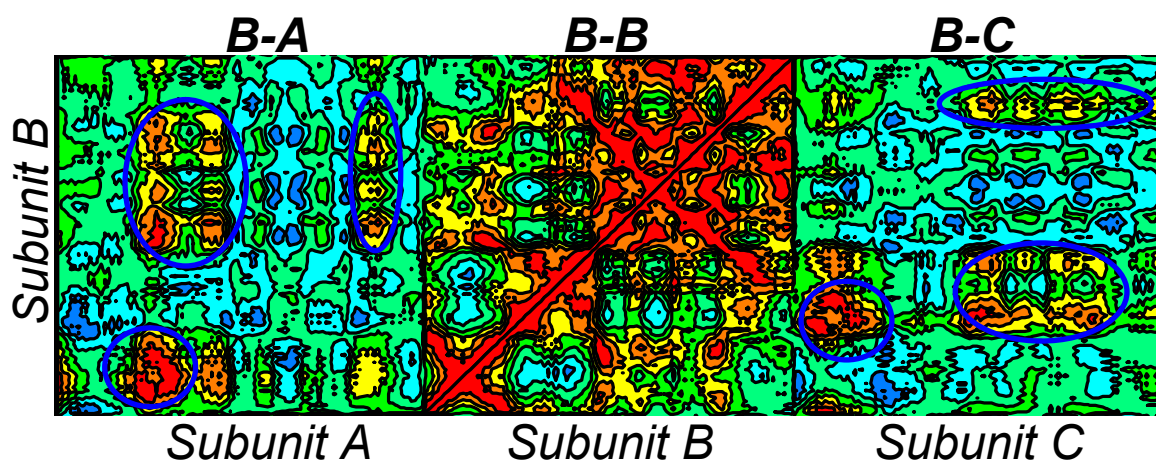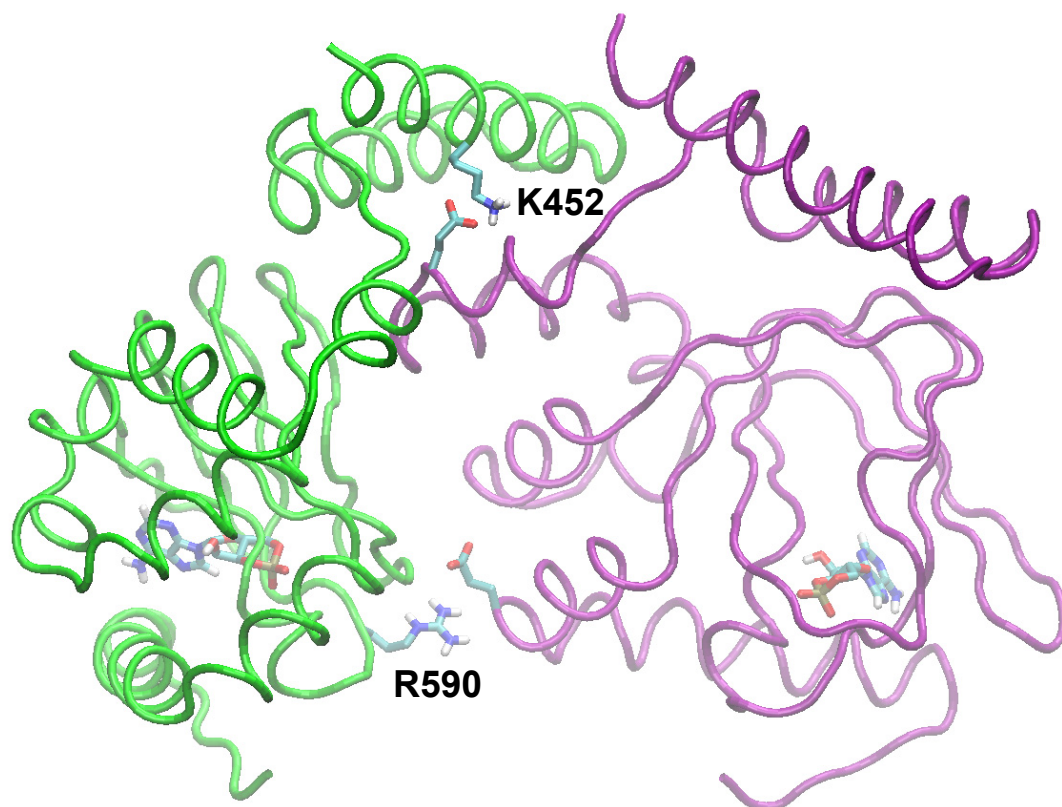

B ANM analysis (eigenvector 6 to 10)
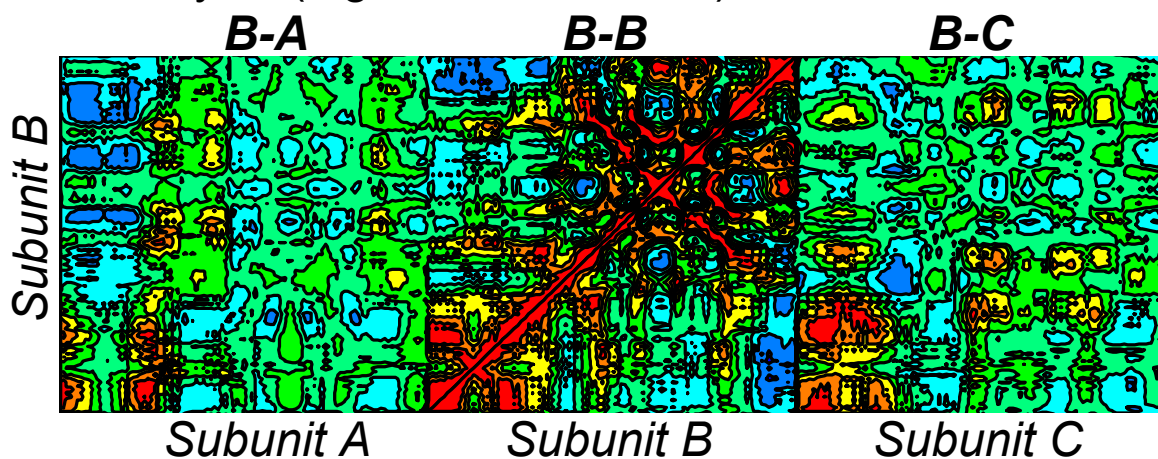
C ANM analysis (eigenvector 11 to 15)
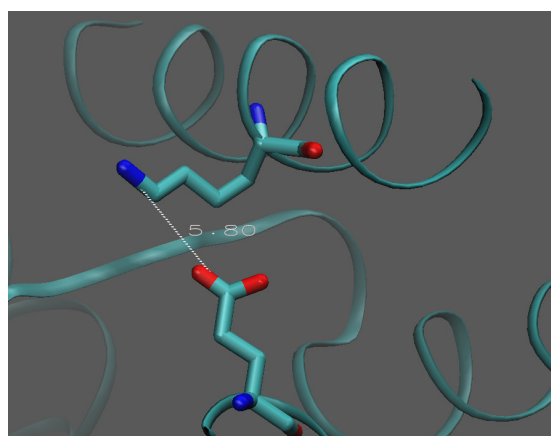
Fig. S2

A Contact map (cut-off 8Å)

B Contact map (cut-off 13Å)

C ANM analysis (cut-off 13Å)

B-A B-B B-C

Subunit B

Subunit A Subunit B Subunit C

A

B K452 – E494
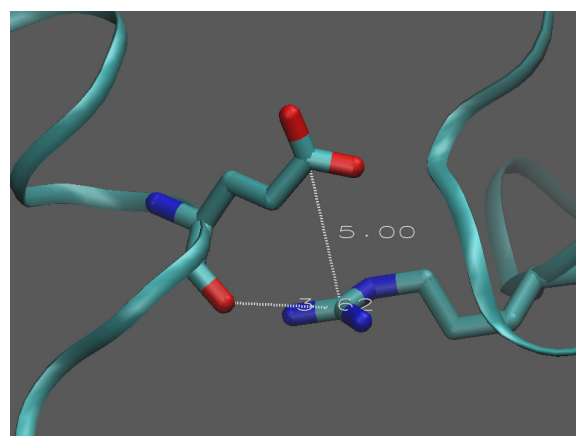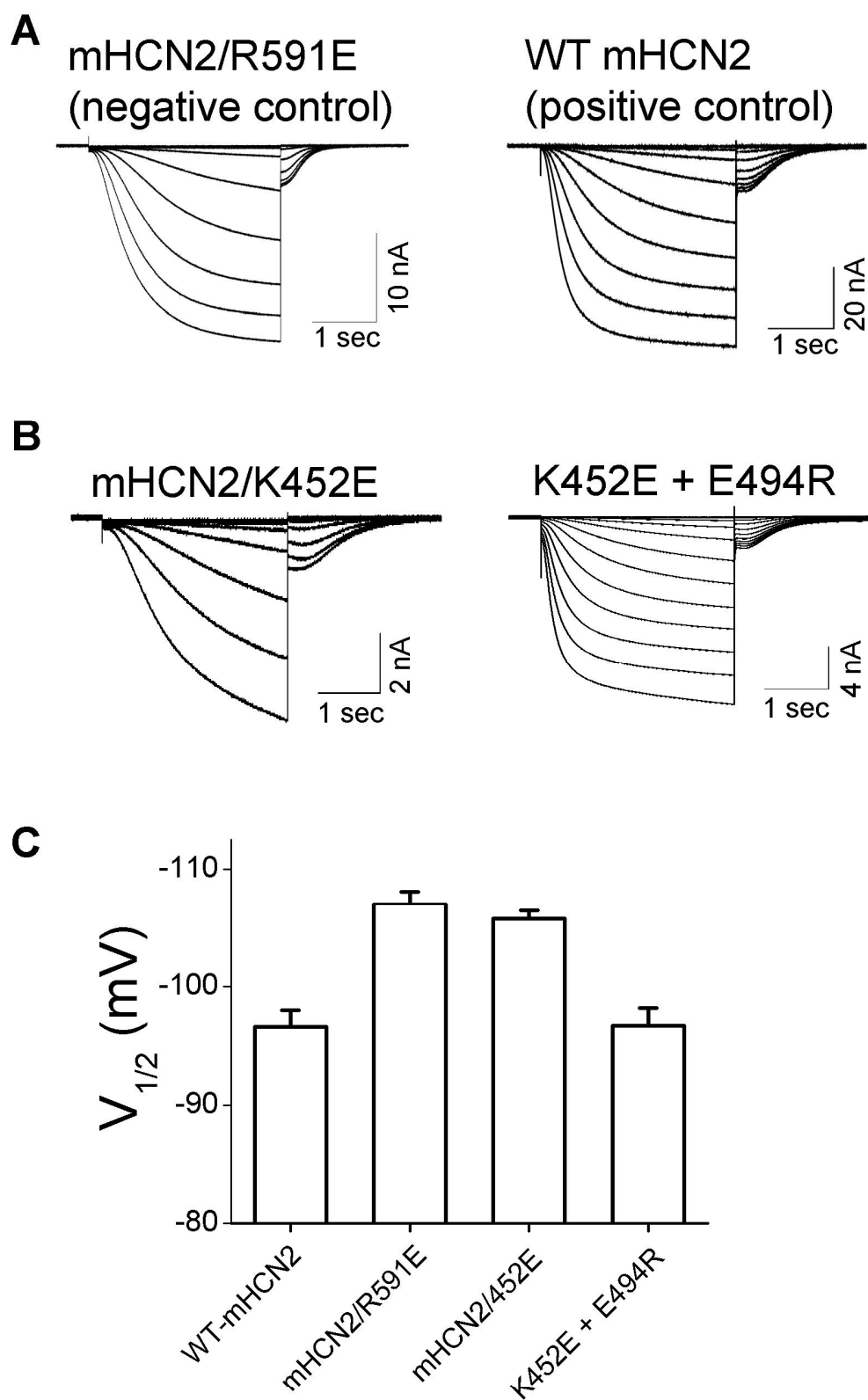

C R590 – E617

Fig. S4

Supplemental Table S1. Summary of TEVC results.

	$V_{1/2}$ (mV)	Activation Time constant (msec) at -120 mV	$\Delta\Delta V_{1/2}$	Deactivation Time constant (msec) at -120 mV
WT-mHCN2	-96.5±1.4	421.3 ±42.4	0	410.6±9.9
R591E	-107±1.1	794.7±60.6	-10.7±2.0	265.4±7.8
K452A	-96.3±1.9	576.1±18.4	2.3±1.9	738.9±33.5
E494A	-85.7±2.7	387.5±56.7	5.2±2.7	542.9±22.9
D522A	no expression	-	-	-
E536A	-83.4±1.4	393.8±32.1	4.4±1.4	671.2±34.0
R546A	-97.1±2.4	663.9±56.4	7.6±2.4	468.6±38.1
K552A	-94.5±2.7	599.1±72.9	-1.7±1.8	440.9±10.8
R590A	-103.8±0.6	719.3±64.8	-11.3±0.6	412.9±4.9
E617A	-96.7±3.1	554.1±36.9	3.4±2.0	486.2±26.4
K452E	-105.6±0.7	1254.6±64.1	-6.9±0.7	546.2±17.4

Supplemental Table S2. Summary of PCF results measured with a -150 mV activation step.

Construct	$\Delta\Delta F$		$\tau_{activation}$ (+150mV)		$\tau_{deactivation}$ (-40 mV)	
	Mean	SE	Mean (sec)	SE	Mean (sec)	SE
WT-mHCN2	0.66	0.05	2.80	0.33	1.01	0.23
K452A	0.58	0.05	2.58	0.16	1.18	0.31
E494A	0.19	0.03	3.17	0.91	1.13	0.14
D522A	-	-	-	-	-	-
E536A	0.31	0.05	4.72	1.64	1.06	0.26
R546A	0.60	0.09	7.08	5.27	0.82	0.15
K552A	0.64	0.08	3.30	0.46	0.84	0.15
R590A	0.18	0.05	1.72	0.65	0.55	0.09
E617A	0.10	0.03	3.17	1.63	1.75	0.47
K452E	0.12	0.03	0.44	0.02	1.68	0.29

References:

1. Zagotta, W. N., N. B. Olivier, K. D. Black, E. C. Young, R. Olson, and E. Gouaux. 2003. Structural basis for modulation and agonist specificity of HCN pacemaker channels. Nature 425:200-205.
2. Sali, A., L. Potterton, F. Yuan, H. van Vlijmen, and M. Karplus. 1995. Evaluation of comparative protein modeling by MODELLER. Proteins 23:318-326.
3. Lindahl, E., B. Hess, and D. van der Spoel. 2001. GROMACS 3.0: a package for molecular simulation and trajectory analysis. Journal of Molecular Modeling [online computer file] 7:306-317.
4. Schuttelkopf, A. W., and D. M. van Aalten. 2004. PRODRG: a tool for high-throughput crystallography of protein-ligand complexes. Acta Crystallogr D Biol Crystallogr 60:1355-1363.
5. Zhou, L., and S. A. Siegelbaum. 2008. Effects of surface water on protein dynamics studied by a novel coarse-grained normal mode approach. Biophys J 94:3461-3474.
6. van der Spoel, D., and P. J. van Maaren. 2006. The Origin of Layer Structure Artifacts in Simulations of Liquid Water. Journal of Chemical Theory and Computation 2:1-11.
7. Atilgan, A. R., S. R. Durell, R. L. Jernigan, M. C. Demirel, O. Keskin, and I. Bahar. 2001. Anisotropy of fluctuation dynamics of proteins with an elastic network model. Biophys J 80:505-515.
8. Van Wynsberghe, A. W., and Q. Cui. 2006. Interpreting correlated motions using normal mode analysis. Structure 14:1647-1653.
9. Ichiye, T., and M. Karplus. 1991. Collective motions in proteins: a covariance analysis of atomic fluctuations in molecular dynamics and normal mode simulations. Proteins 11:205-217.
10. Xu, X., Z. V. Vysotskaya, Q. Liu, and L. Zhou. 2010. Structural basis for the cAMP-dependent gating in the human HCN4 channel. J Biol Chem 285:37082-37091.
11. Wu, S., Z. V. Vysotskaya, X. Xu, C. Xie, Q. Liu, and L. Zhou. 2011. State-dependent cAMP binding to functioning HCN channels studied by patch-clamp fluorometry. Biophys J 100:1226-1232.
12. Seifert, R., A. Scholten, R. Gauss, A. Mincheva, P. Lichter, and U. B. Kaupp. 1999. Molecular characterization of a slowly gating human hyperpolarization-activated channel predominantly expressed in thalamus, heart, and testis. Proc Natl Acad Sci U S A 96:9391-9396.
13. Santoro, B., S. Chen, A. Luthi, P. Pavlidis, G. P. Shumyatsky, G. R. Tibbs, and S. A. Siegelbaum. 2000. Molecular and functional heterogeneity of hyperpolarization-activated pacemaker channels in the mouse CNS. J Neurosci 20:5264-5275.